Cell

Structural Basis for Activation of the Receptor Tyrosine Kinase KIT by Stem Cell Factor

Satoru Yuzawa,[1,2] Yarden Opatowsky,[1,2] Zhongtao Zhang,[1,3] Valsan Mandiyan,[1] Irit Lax,[1] and Joseph Schlessinger[1,*]
[1] Department of Pharmacology, Yale University School of Medicine, 333 Cedar Street, New Haven, CT 06520, USA
[2] These authors contributed equally to this work.
[3] Present address: Department of Biochemistry, New York Medical College, Valhalla, NY 10595, USA.
*Correspondence: joseph.schlessinger@yale.edu
DOI 10.1016/j.cell.2007.05.055

SUMMARY

Stem Cell Factor (SCF) initiates its multiple cellular responses by binding to the ectodomain of KIT, resulting in tyrosine kinase activation. We describe the crystal structure of the entire ectodomain of KIT before and after SCF stimulation. The structures show that KIT dimerization is driven by SCF binding whose sole role is to bring two KIT molecules together. Receptor dimerization is followed by conformational changes that enable lateral interactions between membrane proximal Ig-like domains D4 and D5 of two KIT molecules. Experiments with cultured cells show that KIT activation is compromised by point mutations in amino acids critical for D4-D4 interaction. Moreover, a variety of oncogenic mutations are mapped to the D5-D5 interface. Since key hallmarks of KIT structures, ligand-induced receptor dimerization, and the critical residues in the D4-D4 interface, are conserved in other receptors, the mechanism of KIT stimulation unveiled in this report may apply for other receptor activation.

INTRODUCTION

Stem cell factor (SCF) is a cytokine that mediates its diverse cellular responses by binding to and activating the receptor tyrosine kinase (RTK) KIT (also known as SCF receptor). KIT was initially discovered as an oncogene in a feline retrovirus that captured an activated and truncated form of the surface receptor (Besmer et al., 1986). SCF is encoded by the murine *steel (Sl)* locus while KIT is encoded by the *dominant white spotting (W)* locus in the mouse (Copeland et al., 1990; Huang et al., 1990; Flanagan and Leder, 1990; Tan et al., 1990; Bernstein et al., 1990). SCF functions as a noncovalent homodimer, and both membrane-anchored and soluble forms of SCF generated by alternative RNA splicing and by proteolytic processing have been described (reviewed in Ashman, 1999). KIT is a member of the type III family of RTKs, which also includes PDGF-receptor-α and β, CSF-1 receptor (also known as M-CSF receptor or FMS), and the FLT3 receptor (also known as FLK2) (reviewed in Ullrich and Schlessinger, 1990; Blume-Jensen and Hunter, 2001). KIT is composed of a glycosylated extracellular ligand-binding domain (ectodomain) that is connected to a cytoplasmic region by means of a single transmembrane (TM) domain (reviewed in Schlessinger, 2000). The ectodomain of KIT and other members of type III RTKs all contain five Ig-like domains, in which the second and third membrane distal domains were shown to play a role in ligand recognition (reviewed in Ullrich and Schlessinger, 1990). Other RTKs whose extracellular ligand-binding domains are composed exclusively of multiple Ig-like repeats include members of the VEGF receptor family (7 Ig-like), CCK4 receptor (7 Ig-like), and FGF receptors (3 Ig-like). The cytoplasmic region of KIT contains a protein tyrosine kinase (PTK) domain with a large kinase-insert region, another hallmark of type III RTKs. Binding of SCF to KIT leads to receptor dimerization, intermolecular autophosphorylation, and PTK activation. It was proposed that the fourth Ig-like domain of KIT is responsible for KIT dimerization in response to either monovalent or bivalent SCF binding (Lev et al., 1992; Blechman et al., 1995). However, other studies have demonstrated that ligand-induced dimerization of KIT is driven by bivalent binding of SCF (Philo et al., 1996; Lemmon et al., 1997).

Characterization of mice mutated at the *Scf* or *Kit* loci has shown that SCF and KIT are required for development of hematopoietic cells, melanocytes, germ cells, and intestinal pacemaker cells (reviewed in Ashman, 1999). In humans, loss-of-function mutations in *KIT* cause the piebald trait that is characterized by depigmentation of the ventral chest and abdomen, white fareflock of hair, deafness, and constipation (Fleischman et al., 1991). A variety of gain-of-function mutations in *KIT* were found in different types of human cancers. Activating *KIT* mutations were found in gastro-intestinal-stromal tumors

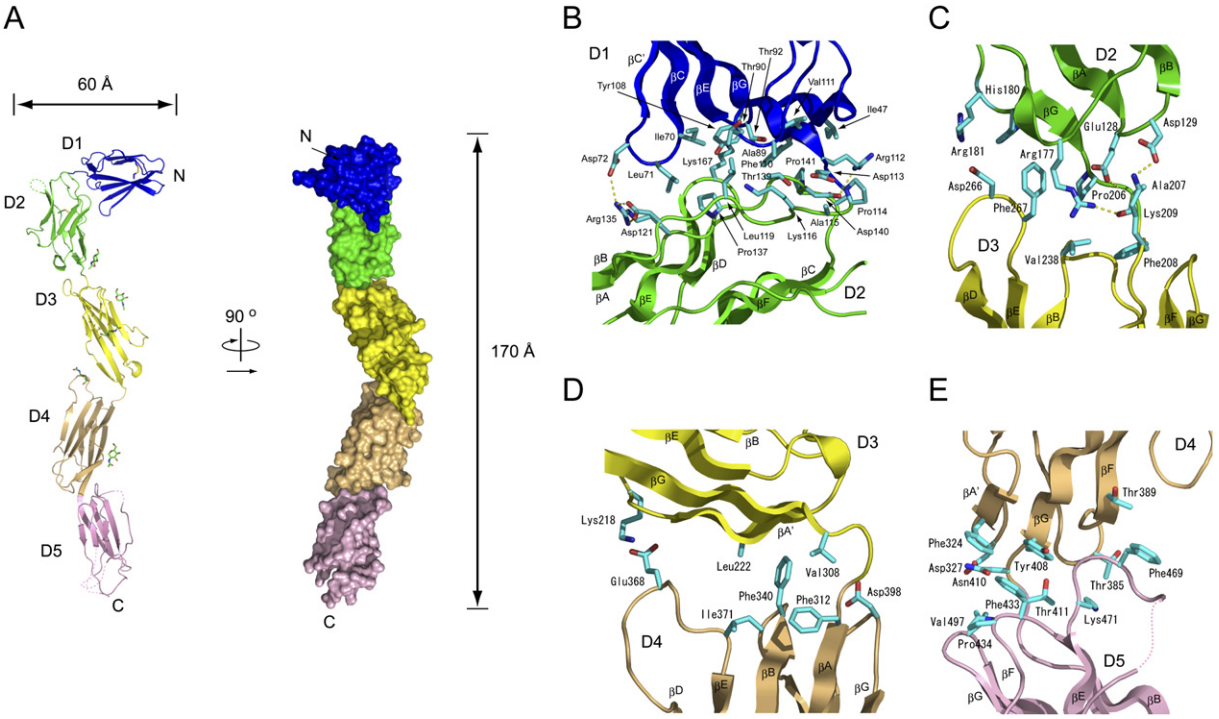

Figure 1. Crystal Structure of KIT Ectodomain

(A) Ribbon diagram (left) and surface representation (right) of KIT ectodomain monomer. Right panel shows a view following 90° rotation along the vertical axis of the view shown in the left panel. D1 is colored in blue, D2 in green, D3 in yellow, D4 in orange, and D5 in pink; N and C termini are labeled. Disulfide bonds in D1 and D5 are shown in ball-and-stick rendering with sulfur atoms colored in orange. Asparagine-linked carbohydrates are shown in a stick model.

(B–E) Detailed views of D1-D2 (B), D2-D3 (C), D3-D4 (D), and D4-D5 (E) interfaces. Color coding is the same as in (A). Amino acids that participate in domain-domain interactions are labeled and hydrogen bonds are drawn as dashed yellow lines. Secondary structure elements are designated according to IgSF nomenclature.

(GIST), acute myeloid leukemia (AML), and mast cell leukemia (MCL), among other cancers. Mutations were identified in the membrane-proximal Ig-like domain (D5) (exons 8 and 9), in the juxtamembrane (JM) domain (exon 11), and in the tyrosine kinase (PTK) domain (exon 17) (reviewed in Forbes et al., 2006). While there is good evidence that the gain-of-function mutations in the JM and the PTK domains lead to constitutive activation of KIT, by relieving autoinhibitory constraints (Mol et al., 2004), the molecular mechanism underlying the gain-of-function mutations in D5 of the ectodomain is not understood.

In this report we describe the crystal structures of the entire ectodomain of KIT in both monomeric and SCF-induced homodimeric (SCF-KIT 2:2 complex) forms. Detailed views of the unoccupied monomeric form at 3.0 Å resolution and SCF-induced homodimeric form at 3.5 Å resolution provide novel insights concerning the activation mechanism of KIT and other RTKs.

RESULTS AND DISCUSSION

The entire ectodomain of KIT composed of five Ig-like domains designated D1, D2, D3, D4, and D5 was expressed in insect cells using the baculovirus expression system. Purified KIT ectodomain monomers or SCF-induced KIT ectodomain homodimers (SCF-KIT 2:2 complex) were each subjected to extensive screening for crystal growth and optimization followed by determination of their crystal structures (Experimental Procedures and Supplemental Experimental Procedures available with this article online).

Structure of the KIT Ectodomain

KIT ectodomain shows an elongated serpentine shape with approximate dimensions of 170 × 60 × 50 Å (Figure 1A). D1, D2, D3, D4, and D5 domains of KIT exhibit a typical immunoglobulin super family (IgSF) fold, composed of eight β strands, designated ABCC′DEFG, assembled into a β sandwich consisting of two antiparallel β sheets (Figure 1A). D1, D2, D3, and D5 each contain a conserved disulfide bond connecting cysteine residues at B5 and F5 (Fifth amino acids of strand B and F, respectively), positions that bridge the two β sheets to form the center of the hydrophobic core of the Ig-like fold (Harpaz and Chothia, 1994). D2 and D5 contain two disulfide bonds and D4 does not contain any cysteine residue; nevertheless, the integrity of the Ig-like fold of D4 is maintained even though the conserved cysteine residues at

B5 and F5 are replaced by a valine and phenylalanine residues, respectively.

The angle between D1 and D2 along the axis of the two domains is 76° (Figures 1A and 1B), resembling the orientation between the first and second Ig-like domains of the interleukin-1β receptor (Vigers et al., 1997). In contrast, the angle between D2 and D3 is 150°, between D3 and D4 is 119°, and between D4 and D5 is 162°. The orientation between the ABED and A′GFC β sheets for the different Ig-like domains are ~180° for D1-D2, ~180° for D2-D3, ~90° for D3-D4, and ~180° for D4-D5 (Figure 1).

The superposition of all five Ig-like domains of KIT ectodomain with telokin (Holden et al., 1992) used as a standard for Ig-folds reveals root-mean-square deviations (rmsd) of 1.5–2.9 Å for equivalent Cα atoms. D2 is the most divergent among the five KIT Ig-like domains (Figure S1) as revealed by its higher rmsd values when superimposed with telokin. Based on structural conservation of key amino acids in Ig-like domains and their secondary structural topology (Harpaz and Chothia, 1994; Halaby et al., 1999), D1, D2, D3, and D4 belong to the I-subset and D5 is related to the C2 and IgCAM subsets of IgSF (see Supplemental Data). Furthermore, among the structurally conserved 20 finger-print residues of IgSF (Harpaz and Chothia, 1994), 10–14 residues are conserved in the five Ig-like domains of KIT (Table S1).

Inter Ig-like Domain Interactions in KIT Monomeric Form

The interdomain interactions between the five Ig-like domains of KIT are responsible for maintaining the overall topology of KIT ectodomain monomers (Figure 1). The orientation of D1 relative to D2 is determined by the extensive buried surface area that is caused by the numerous interactions between the two Ig-like domains (Figure 1B). The buried surface area of 1240 Å^2 in the D1-D2 interface is much larger than the buried surface areas of most inter Ig-like domain interfaces of rod-like multidomain IgSF structures (Su et al., 1998) including the three other inter Ig-like interfaces in the KIT ectodomain that range between 500 and 800 Å^2. This interface is formed primarily by hydrophobic and electrostatic interactions between strands A′ and G, loops EF and CC′ of D1 with the N-terminal region of strand A, the C-terminal end of strand B, and loops BC and DE of D2 (Figure 1B and Supplemental Data). Moreover, many residues in the D1-D2 interface including amino acids from strands G of D1, the linker region connecting D1 and D2, and the BC loop of D2 are conserved in KIT from different species (Figure 1B).

The buried surface area of the D2-D3 interface is approximately 780 Å^2. The D2-D3 interface is composed of a small hydrophobic patch surrounded by two electrostatic interactions. This interface is formed by interaction between the EF loop of D2 and the DE loop of D3 and interactions between the D2-D3 linker region and the FG and BC loops of D3 (Figure 1C and Supplemental Data). The buried surface area of the D3-D4 interface is approximately 570 A^2. D3 and D4 interact primarily through strands A′ and G of D3 with the BC and DE loops of D4 (Figure 1D and Supplemental Data). The length of the D3-D4 interface is approximately 20 Å due to the angular arrangement of D4 relative to D3 with an angle of 119° along the long axis of the two Ig-like domains. The D4-D5 interface forms a buried surface area of 760 Å^2, mainly mediated by hydrophobic interactions (Figure 1E). The interface is formed by interactions between strands A, G, and F of D4, with the BC and DE loops of D5, as well as with the D4-D5 linker region (Figure 1E and Supplemental Data).

Overall Structure of the SCF-KIT Complex

The structure of SCF-KIT complex shows 2:2 stoichiometry, in which two sets of 1:1 complexes in the asymmetric unit are related by a noncrystallographic 2-fold symmetry (Figure 2). The observed SCF-KIT 2:2 complex in the crystal lattice is consistent with experiments demonstrating that KIT dimerization is driven by the dimeric SCF ligand (Philo et al., 1996; Lemmon et al., 1997). The two sets of KIT ectodomains and SCF molecules resemble an upside down "A" letter with approximate dimensions of 170 × 130 × 70 Å (Figure 2A and Figure S2).

The overall structure of SCF bound to KIT is similar to the previously described structures of free SCF (Zhang et al., 2000; Jiang et al., 2000). The structure of SCF-KIT 2:2 complex shows that an individual SCF protomer binds directly to D1, D2, and D3 of an individual KIT protomer (Figure 2B). Consequently, a single-receptor protomer forms a symmetric complex with a similar 2-fold related surface on an SCF protomer. Dimerization of KIT is also mediated by homotypic interactions between the two membrane-proximal Ig-like domains of KIT, namely by D4-D4 and D5-D5 interactions (Figure 2B). This results in dramatically altered configurations of D4 and D5 relative to the rest of the molecule, and these configurations bring the C termini within 15 Å of each other close to the place where they connect to the transmembrane domain (Figures 2B and S2). The structure is also characterized by the existence of a large cavity at the center of the complex with dimensions of ~50 × 50 × 15 Å (Figure 2B). The crystal structure demonstrates that each protomer of SCF binds exclusively to a single KIT molecule and that receptor dimerization is driven by SCF dimers that facilitate additional receptor-receptor interactions.

SCF-Binding Region of KIT

SCF is bound to a concave surface formed by D1, D2, and D3 of KIT in a configuration in which the four-helix bundle of SCF is oriented perpendicularly to the long axis of D1, D2, and D3 and the C termini of SCF and KIT are facing opposite directions (Figures 2, 3, and S2). The solvent-accessible surface area buried at the interface between KIT and each SCF protomer is approximately 2060 Å^2, a buried surface area that is within the range of known ligand-receptor interfaces. It is possible to divide the SCF-KIT interface into three binding sites (Figures 3A

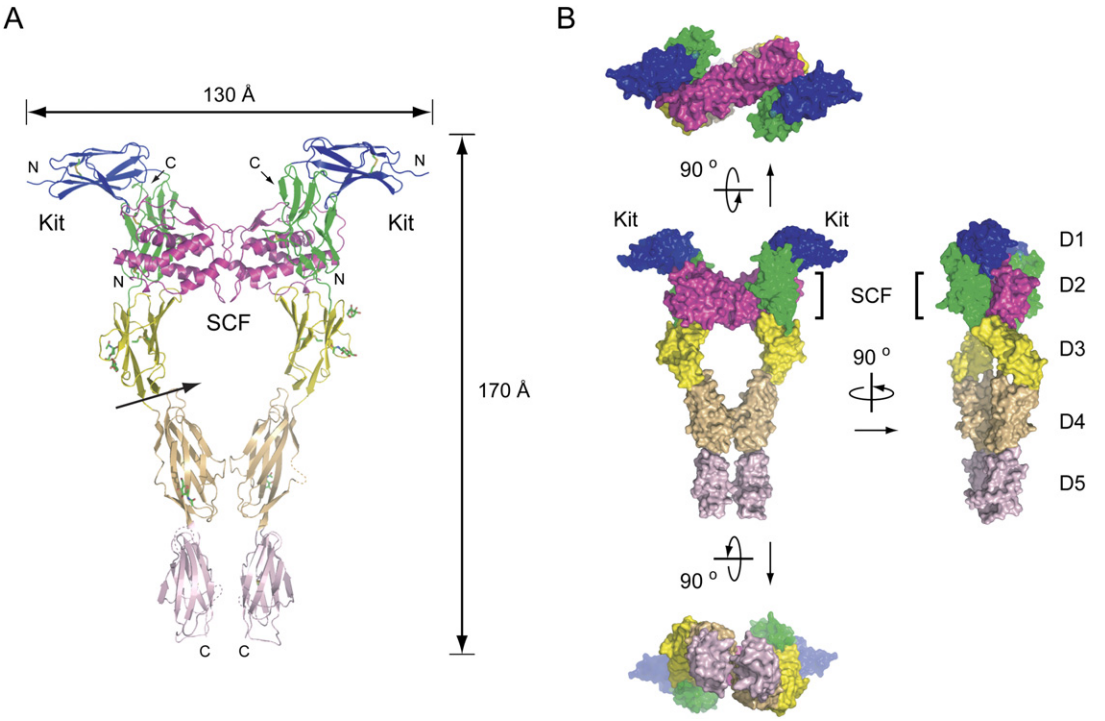

Figure 2. Crystal Structure of the SCF-KIT Ectodomain 2:2 Complex

(A) Ribbon diagram of the SCF-KIT 2:2 complex. Color coding of D1 to D5 is the same as in Figure 1 and SCF is colored in magenta. N and C termini of KIT and SCF are labeled. Disulfide bonds in D1 and D5 are shown in ball-and-stick rendering with sulfur atoms colored in orange. Asparagine-linked carbohydrates are represented in a stick model. Arrow marks a large cavity in the SCF-KIT 2:2 complex. (See stereo view in Figure S2.)

(B) Surface representations of the SCF-KIT ectodomain 2:2 complex. The figures show a top view (top), face view (center left), side view (center right), and bottom view (low). Color coding is the same as in (A). The views show that a SCF dimer interacts symmetrically with D1, D2, and D3 of two corresponding KIT ectodomains. In addition, KIT ectodomains form homophylic interactions through lateral contacts between D4 (orange) and between D5 (pink) of two neighboring receptors.

and 3B and Table S2). Site I is located in D1, site II is located in D2 and in the D2-D3 linker region, and site III is located in D3. The buried surface areas of sites I, II, and III are approximately 280, 770, and 1010 Å^2, respectively.

Site I

The αC-β2 loop of SCF is aligned perpendicularly to strand C′ of D1, as presented in Figure 3C. Asp72, Glu73, and Thr74 of D1 and Lys99′, Ser101′, and Phe102′ of SCF are closely located at a Cα distance of 6–8 Å, indicating that these residues could participate in the interactions between D1 and SCF. Due to poor side-chain electron density of the αC-β2 loop, specific interactions could not be defined.

Site II

SCF binding is mediated, for the most part, by complimentary electrostatic interactions of charged surfaces on KIT (Figures 3A, 3B, and 3D). Salt bridges are formed between the basic amino acids Arg122, Arg181, Lys203, and Arg205 of KIT with the acidic amino acids Asp54′, Asp77′, Asp84′, and Glu88′ on SCF. The conformation of Arg122 is stabilized by the salt bridge between Glu198 of KIT and Asp54′ of SCF. Figure 3D shows that three of the major interacting residues, Tyr125, Arg181, and Lys203, on D2 are aligned on the same plane and form hydrogen bonds with Asp77′, Asn81′, Asp84′, Ser53′, and Thr57′ of αB and αC of SCF. The van-der-Waals contacts between Ser123 and Ile201 of D2 and Val50′ and Thr57′ of SCF also contribute to the formation of a ligand-receptor complex. However, there are notable differences in residues of site II in KIT and SCF from other species (Figures 3, S1, and S3). While Arg181 and Lys203 are invariant as basic amino acids in mammals, Tyr125 is substituted by a phenylalanine in mouse and rat, which most likely results in loss of a hydrogen bond. Arg205 of KIT is a highly conserved amino acid while Glu88′ is substituted for by leucine and alanine residues in mouse and rat, respectively. Furthermore, Arg122 of KIT and Asp54′ of SCF in human are substituted by a leucine or valine in mouse and rat, respectively. These substitutions may account for the reduced affinity of rodent SCF toward human KIT (Lev et al., 1992).

Site III

The N-terminal segment of SCF interacts with strand D of D3 (Figures 3A and 3E). Hydrogen bonds are formed between the side chain of Asn10′ of SCF and the main-chain

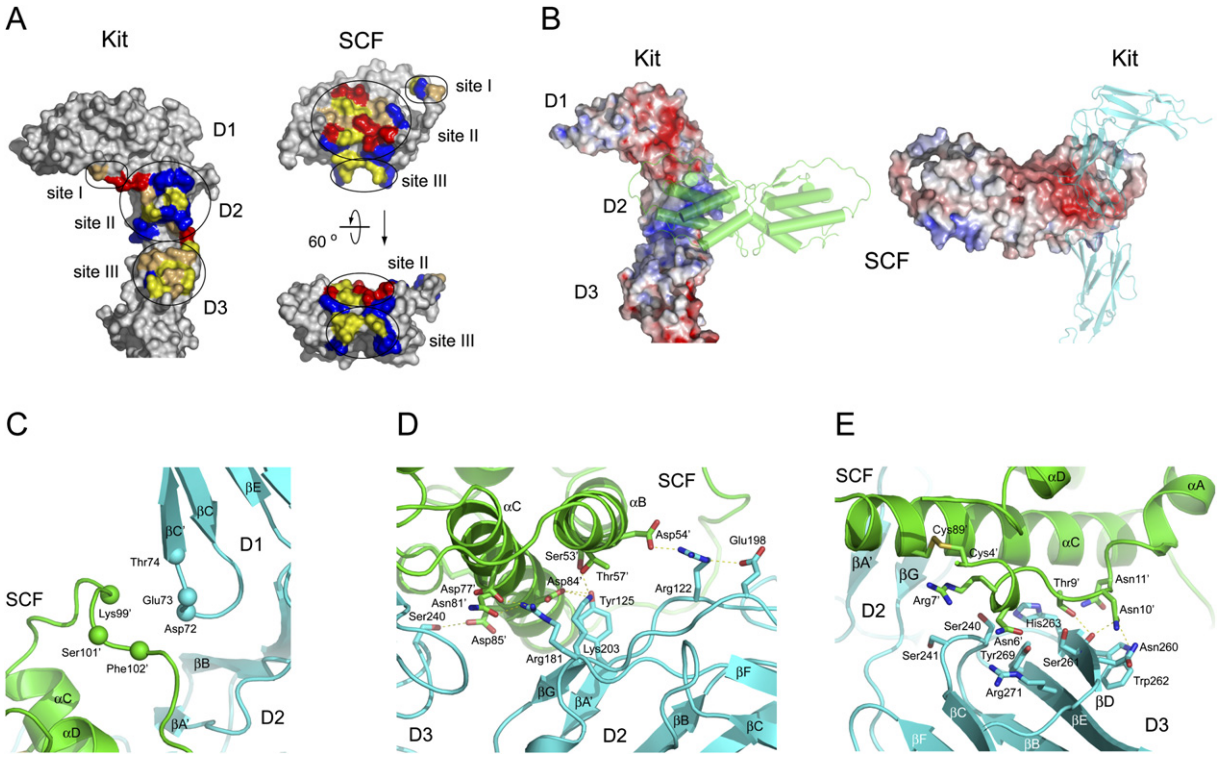

Figure 3. SCF Recognition by KIT

(A) Views of the SCF-KIT interface. Amino acids in the buried surfaces in SCF and KIT ectodomain are visualized by pulling apart the two molecules. The figure shows the molecular surface of KIT D1-D2-D3 (left) and SCF (right). Acidic amino acids are shown in red, basic amino acids in blue, polar amino acids in orange, and hydrophobic amino acids in yellow. SCF binding site I, site II, and site III on KIT are circled.

(B) Complementarity in electrostatic potential in the ligand-receptor interface. The right panel shows a view following a rotation of 180° along the vertical axis of the electrostatic surface presented in the left panel. Electrostatic surface potential of D1-D2-D3 superimposed on the molecular surfaces with an imprint of a cartoon diagram of bound SCF that is colored in green is shown. Right panel depicts the electrostatic surface potential of SCF-bound KIT colored in blue (positive) and red (negative). KIT is shown in a form of ribbon diagram colored in cyan.

(C–E) Close-up views of site I (C), site II (D), and site III (E) of the SCF-KIT interface. SCF is colored in green and KIT in cyan. Interacting amino acids are labeled, hydrogen bonds are drawn as dashed yellow lines, and secondary structure elements are marked on the ribbons and strands.

amide and carbonyl group of Ser261, as well as with the side chain of Asp260 and Trp262 on D3. In addition, Thr9′ and Asn11′of SCF bind to the side-chain and main-chain amides of Ser261 and His263 of KIT, respectively. Mutational analysis of SCF has shown that replacement of Asn10′ with alanine or glutamic-acid residues reduces the binding affinity of SCF toward KIT by approximately 10-fold and that Asn10′ (or Asp in other species) is necessary for biological activity (Hsu et al., 1998). Comparison of the receptor-binding interface in SCF from different species shows that Asn10′ (or Asp) is a highly conserved residue (Figure S1). Additional important interactions are mediated by Asn6′ and Arg7′ of SCF via van-der-Waals contacts with Tyr259, Thr269, Ser240, Val242, Ser241, and Ser244 on D3 of KIT.

The Ligand-Binding Domain of KIT Is Poised for SCF Binding

Superimposition of the structures of individual D1, D2, and D3 of KIT monomeric form with corresponding structures of the SCF-induced homodimeric form reveals rmsd values of 0.5, 0.8, and 1.1 Å for 82, 92, and 100 aligned Cα residues in D1, D2, and D3, respectively. Similarly, superimposition of the structure of the entire D1-D2-D3 region of KIT monomers with the corresponding structures in the SCF-KIT 2:2 complex reveals an rmsd of 1.1 Å for 274 aligned Cα residues of the D1-D2-D3 region. Remarkably, there are no significant backbone changes in the structures of the SCF-binding pocket of KIT (Figures 3 and S4). However, several minor structural changes were detected in the SCF-binding cleft upon SCF binding. A structural change is seen in the top half of strands G, F, and C (amino acids 167–187 and 143–166) of D2 following SCF binding (Figures 1A and 2A). These strands are located at the side opposite to the SCF-binding interface and are not involved in mediating any direct contacts with SCF. Overall, comparison of the structures of KIT monomers to those of SCF-occupied KIT dimers show that the D1-D2-D3 region of KIT may be viewed as a functional unit that is poised for SCF binding followed by

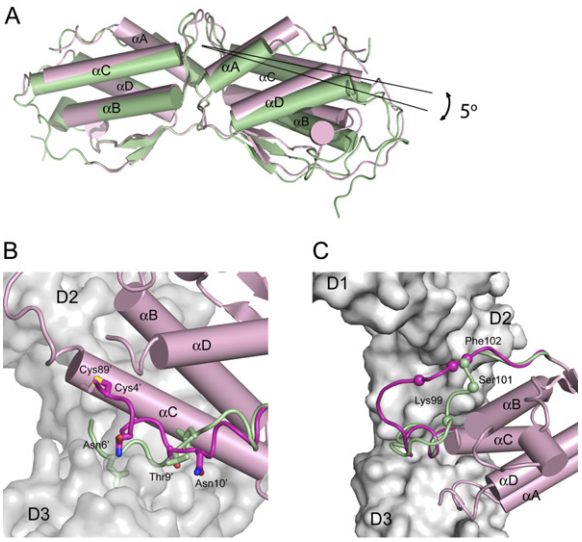

Figure 4. Conformational Changes in SCF upon Binding to KIT

(A) The angle between the two SCF protomers is altered upon KIT binding. The view shows a cartoon diagram of free SCF (green) (Zhang et al., 2000) and SCF bound to KIT (magenta). Superimposition of the one SCF protomer (left) reveals an angular movement of approximately 5° of the second protomer (right), as measured for helix αC. Helices are labeled and shown as cylinders.

(B) Conformational change in the N terminus of SCF upon KIT binding. Site III of KIT is shown as a molecular surface (gray), and the N terminus of free SCF is shown in green and of SCF bound to KIT in magenta. Disulfide bond between Cys4′ and Cys89′ is shown as a yellow stick. Key amino acids are labeled and shown as a stick model.

(C) Conformational change in αC-β2 loop of SCF upon binding to site I of KIT. Color coding is the same as in (B).

subsequent KIT dimerization driven by dimeric SCF molecules.

Conformational Changes in SCF Molecules Bound to KIT

While the overall structure of SCF bound to KIT is similar to the structure of free SCF, there are notable differences in the angle between the two protomers, in the conformations of the connecting loops, and in the structures of the flexible N terminus of the molecule (Figure 4). Comparison of the published structures of SCF dimers (entries 1EXZ and 1SCF in the Protein Data Bank [PDB]) shows that the angle between the two protomers (the angles between αC helices) of free SCF homodimers may vary by 2° to 6° in the different structures, suggesting that a certain degree of flexibility exists in the SCF dimer. The range of differences in the angles between KIT-bound SCF protomers to those of free SCF was increased by 3°–9°. Figure 4 shows a KIT-bound SCF structure in which the angle between SCF protomers is increased by 5°. Interestingly, it was shown that the flexibility of the cytokine activin plays a role in the assembly of TGF-β receptors (Greenwald et al., 2004).

Figure 4B shows that the N terminus of free SCF from Cys4′ to Asn11′ has a random-coil configuration (Zhang et al., 2000). It was also shown that deletion of the first four amino acids leads to approximately 25% reduction in the binding affinity of SCF to KIT, suggesting that the disulfide bridge between Cys4′ and Cys89′ plays a role in maintaining the functional integrity of SCF (Langley et al., 1994). Figure 4B also shows that Thr9′ and Asn10′ of the N terminus region of SCF bound to KIT undergo a conformational change in which their Cα positions become displaced by 3 to 5 Å upon receptor binding (Figure 4B). The disulfide bridge between Cys4′ at the N terminus and Cys89′ at the αC helix appears to play an important role in mediating the conformational change that takes place in the N terminus of SCF. The position of Cys24′ in free SCF is not altered upon receptor occupancy as revealed by an rmsd of 1.2 Å of Cα positions. Finally, The αC-β2 loop of free SCF is either disordered or has a different structure from the structure of the αC-β2 loop in SCF bound to KIT. Figure 4C shows that the αC-β2 loop of SCF undergoes a large conformational change upon receptor binding, a change critical for establishment of site I of the SCF-KIT interface.

A Large Rearrangement in D4 and D5 Orientations in SCF-Bound KIT

Superimposition of the structures of individual D1, D2, D3, D4, and D5 of KIT monomeric form with corresponding individual Ig-like domains in the SCF-induced homodimeric form reveals minor changes in the structure of KIT Ig-like domains following SCF binding. By contrast, superimposition of the D3-D4-D5 region of KIT monomeric form with the corresponding region in the homodimeric form reveals a large structural change in the orientation of D4 and D5 relative to each other and relative to the ligand-binding region of KIT (Figures 5A and S5). Each of the individual domains D3, D4, and D5 of monomeric KIT can be superimposed with their counterparts in the SCF-occupied KIT with rmsd values of 0.9, 0.9, and 1.9 Å for 98, 101, and 85 Cα atoms of D3, D4, and D5, respectively. However, superimposition of D3 structure of KIT monomers with D3 structure in ligand-occupied homodimeric form reveals a dramatic movement in the orientation of D4 and D5 in SCF-bound KIT (Figure 5A). The reorientations of D4 and D5 relative to the ligand-binding region occurs by a rotation along an axis in the linker connecting D3 to D4 and a rotation along an axis in the linker connecting D4 to D5 running through the D3-D4 and D4-D5 interfaces (Figure 5A), respectively. Comparison of the free and ligand-bound KIT shows that D4 of ligand-occupied KIT rotates relative to D3 by 22°, and D5 of ligand-occupied KIT rotates relative to D4 by 27° (Figure 5A). The rearrangements of D4 and D5 in SCF-occupied KIT result in receptor-receptor interactions that are mediated by D4-D4 and D5-D5 interactions of two neighboring KIT molecules (Figure 5B). The conformation of the DE loop of D5 is altered in SCF-occupied ectodomain.

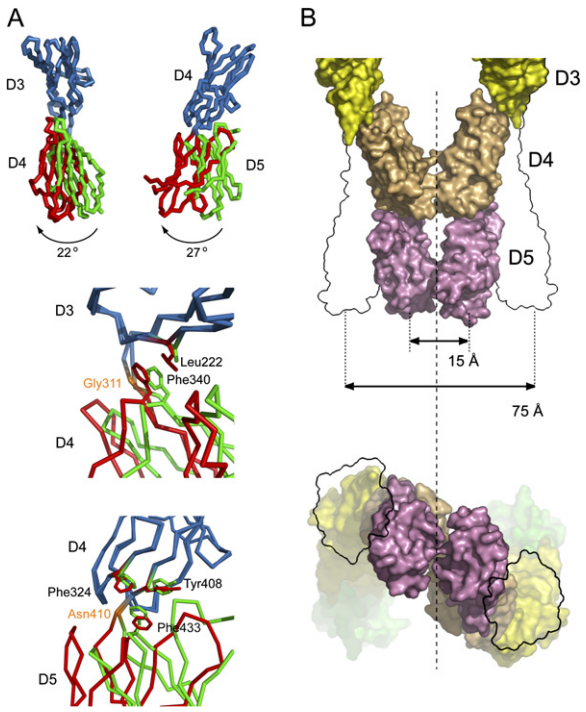

Figure 5. Reconfiguration of KIT D4 and D5 upon SCF Binding

(A) Reconfiguration of D4 and D5 in the SCF-KIT complex. Superimposition of D3 from the KIT monomer with D3 of KIT bound to SCF (both colored blue) shows that D4 of the bound form (red) moves by 22° relative to the position of D4 of the free form (green). Superimposition (right panel) of D4 of the two forms (both in blue) shows that D5 of the SCF-bound form (red) moves by 27° relative to the positions of D5 of the free form (green). The two bottom panels show close views of the hinge regions of the D3-D4 and D4-D5 interfaces of the monomeric (green) and homodimeric (red) forms.

(B) Surface representation of D4 and D5 of SCF-occupied KIT (top panel), viewed in the same orientation as in Figure 2. The black outline shows the location of D4 and D5 of KIT ectodomain monomers bridged by SCF binding to the ligand-binding region. Reconfiguration of D4 and D5 leads to a movement of the C termini of two neighboring ectodomains from 75 Å to 15 Å from each other. Lower panel shows a view from the cell membrane (bottom view) of the SCF-KIT complex (see Movies S1 and S2). Note a 90° rotation along the *x* axis. Color coding of D1 to D5 is the same as in Figure 1.

Reorientation of D4 and D5 driven by receptor dimerization imposes upon the DE loop of D5 a new configuration (Figure 5A).

D4:D4 Interactions in KIT Homodimers

Homotypic interactions between D4 of two neighboring KIT molecules are mediated by the D4-D4 interface in the SCF-KIT 2:2 complex. The D4-D4 interface is mediated by two β sheets formed by the ABED strands of D4 of each KIT protomer to form a nearly planar arrangement in which Arg381 of each protomer points toward each other resulting in a buried surface area of 360 A^2. Figure 6A shows that Arg381 and Glu386 form salt bridges and vander-Waals contacts across the 2-fold axis of the KIT dimer. In addition, the side chains of Arg381 of each protomer form hydrogen bonds with the main-chain carbonyl of the corresponding residue of the neighboring KIT molecules.

Structure-based sequence analysis has shown that the D4-D4 interface is conserved in most type III RTKs including CSF1R, PDGFRα, and PDGFRβ (Figures 6B and S1). In PDGFRα Glu386 is replaced by an aspartic acid, a residue that could also function as a salt bridge partner. A pair of basic (Arg381) and acidic (Glu386) residues are strictly conserved in type III RTKs of different species. The sequence motif found in the D4-D4 interface is also conserved in the membrane-proximal 7^{th} Ig-like domain (D7) of all members of type V RTKs (VEGFR family) including FLT1 (type 1), FLK1 (type 2), and FLT4 (type 3). In VEGFR, the basic (Arg) and acidic (Asp) residues are located in the EF loop. Although the core sequence motif that is responsible for the D4-D4 interface is located in a different Ig-like domain of VEGFR (i.e., D7 versus D4) it is possible that receptor-receptor interactions similar to those seen in the D4-D4 interface of KIT will also take place through a similar D7-D7 interface (Figure 6A) in all members of the VEGFR family of RTKs (Ruch et al., 2007).

D5-D5 Interactions in KIT Homodimers

Figures 2B, 5B, and 6C show that in the SCF-KIT 2:2 complex neighboring D5 protomers are parallel and in a close proximity to each other as well as in an orientation likely to be perpendicular to the cell membrane. The β sheet topology of D5 follows an atypical arrangement that is different from most I-set IgSF in which strand A is split into strand A and A′ (see also Supplemental Data). Strand A of D5 is paired with strand B resulting in the β sheet topology of ABED/CFG. Consequently, strands A and G that are located at the edge of two β sheets (ABED/CFG) are nearly parallel at a distance of 6.5–11.5 Å in the Cα from each other. Moreover, strands A and G of one protomer face strands A and G of neighboring D5 in a 2-fold symmetry. The side chains of Asn505 of two neighboring KIT protomers are approximately 4.2 Å from each other, but water or metal ions that may mediate indirect interactions between the two asparagines could not be detected in this area of weak electron density. Additional D5-D5 interactions are mediated by Tyr418 of two neighboring KIT molecules (Figure 6C). The interaction between hydroxyl groups of neighboring Tyr418 side chains could be mediated by water molecules. It also suggests that the relative positions of neighboring D5 domains are mediated by indirect interactions formed by Tyr418 and Asn505 of the neighboring protomers. The G strand of D5 is connected via a short linker to the transmembrane domain of KIT.

KIT Mutations in Human Diseases

A variety of human diseases are caused by mutations in the *KIT* gene. In humans, loss-of-function mutations in the ectodomain of KIT cause the piebald trait (Fleischman et al., 1996; Murakami et al., 2005). These exon 2 and exon 3

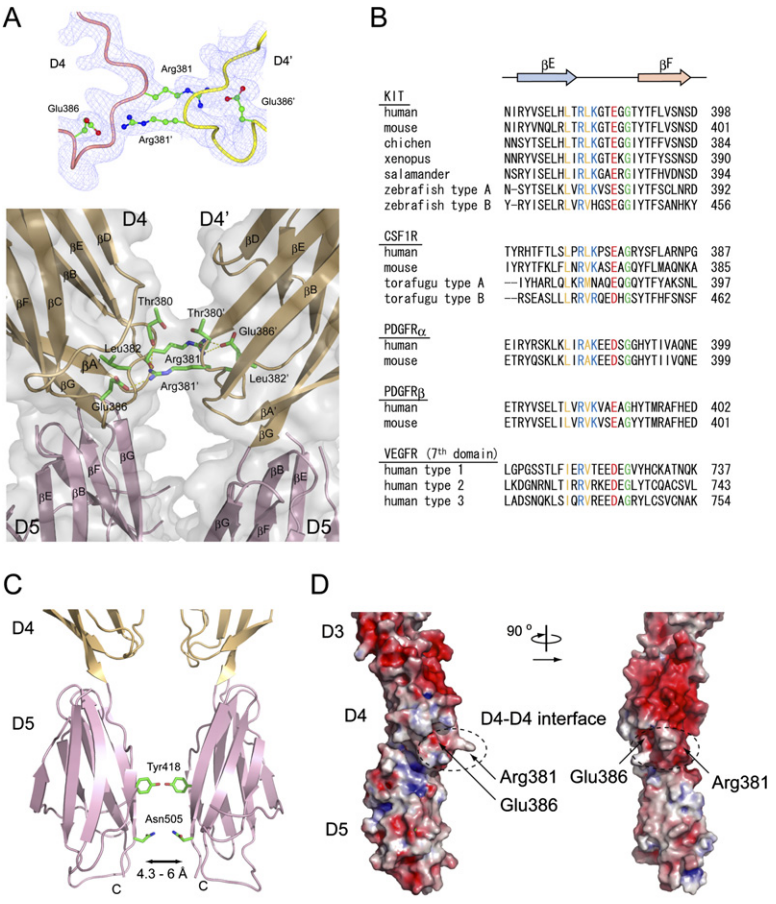

Figure 6. Views of the D4-D4 and D5-D5 Interfaces

(A) 2Fo-Fc electron density map contoured at 1.1σ level showing a view of the D4-D4 interface (top panel). The backbones of KIT protomers are represented as pink and yellow tubes, respectively. A close view (bottom panel) of the D4-D4 interface of two neighboring ectodomains is shown. Interchain hydrogren bonds formed between Arg381 and Glu386 of two adjacent D4 are colored in yellow. Key amino acids are labeled and shown as a stick model. Secondary structure elements are labeled according to the IgSF nomenclature.

(B) Conservation of the D4-D4 dimerization motif across members of type III and type V RTK families. Residues 370–398 of human KIT (AAC50969.1) aligned with sequences of (with accession numbers) mouse (AAH75716.1), chicken (NP_989692.1), *Xenopus laevis* (AAH61947), salamander (AAS91161.1), and zebrafish (type A and B (NP_571128, XP_691901) homologs. Also shown are amino-acid sequences of CSF1R from human (P07333), mouse (P09581), and torafugu type A and B (P79750, Q8UVR8) and sequences from PDGFRα and PDGFRβ from human (P16234, P09619) and mouse (NP_035188, P05622). Amino-acid sequences of type V RTKs of human VEGFR type 1–3 (7^{th} Ig-like domain) (P17948, P35968, and P35916) are also presented. Secondary structure elements on KIT are labeled on the top of the sequence alignment. The conserved residues of Arg381 and Lys383, Leu382 and Leu379, and Glu386 and Gly388 are colored in blue, yellow, red, and green, respectively.

(C) Ribbon diagram of a D5-D5 interface. Strands A and G of two adjacent KIT protomers participate in formation of the D5-D5 interface. The D5-D5 interface is maintained by lateral interactions between Tyr418 and Asn505 of two neighboring receptors probably through ion(s) or water molecule(s).

(D) Electrostatic potential surfaces of D4 and D5 of KIT. The figures show a face view of the D4-D4 interacting surface (right) and a view following 90° rotation along the vertical axis (left). The position of acidic patch and the D4-D4 interfaces are circled and the interacting residue Arg381 and Glu386 are labeled.

point mutations in the *KIT* locus result in Cys136 being replaced by an arginine residue and Ala178 being substituted for by a threonine residue. Both mutations take place in D2, a critical component of the SCF-binding site on KIT (Figure 7A). The piebald Cys136Arg mutation will cause the loss of an important disulfide bond that plays a critical role in maintaining the structural and functional integrity of D2 and hence its capacity to recognize SCF. Ala178 is located in the EF loop of D2 in close proximity to the D2-D3 interface (Figure 7A). The piebald Ala178Thr mutation may disrupt interactions that are essential for maintaining the integrity of the D2-D3 interface and interactions that are required for D2 and/or D3 binding to SCF (Figure 7A).

A variety of gain-of-function mutations in the *KIT* locus were found in different cancers including GIST, AML, and SCLC (reviewed in Forbes et al., 2006). Many oncogenic mutations were identified in the JM and in the PTK domains of KIT. A variety of oncogenic mutations were also found in KIT ectodomain (Figure 7A) including in-frame deletions, point mutations, in-frame duplications, and insertions that collectively lead to formation of activated forms of KIT. In-frame deletion and insertional mutations at exon 8 involving either a loss or substitution of Asp419 were described in patients with AML, while duplications of Ala502-Tyr503 and Ala502-Phe506 sequences were identified in GIST (Figure 7A). Asp419 is located in a region connecting strand A and the AB loop of D5, and Ala502-Tyr503 are located on strand G of D5 of KIT. Interestingly, virtually all the activating oncogenic mutations that were found in KIT ectodomain were mapped to the D5-D5 interface (Figure 7A). The most plausible interpretation of the mode of action of the oncogenic D5 mutations is that these mutations enhance the binding affinity and homotypic interactions between neighboring D5 domains by increasing the on-rate or decreasing the off-rate or altering the rates of both processes in a fashion that facilitates enhanced D5-D5 interactions.

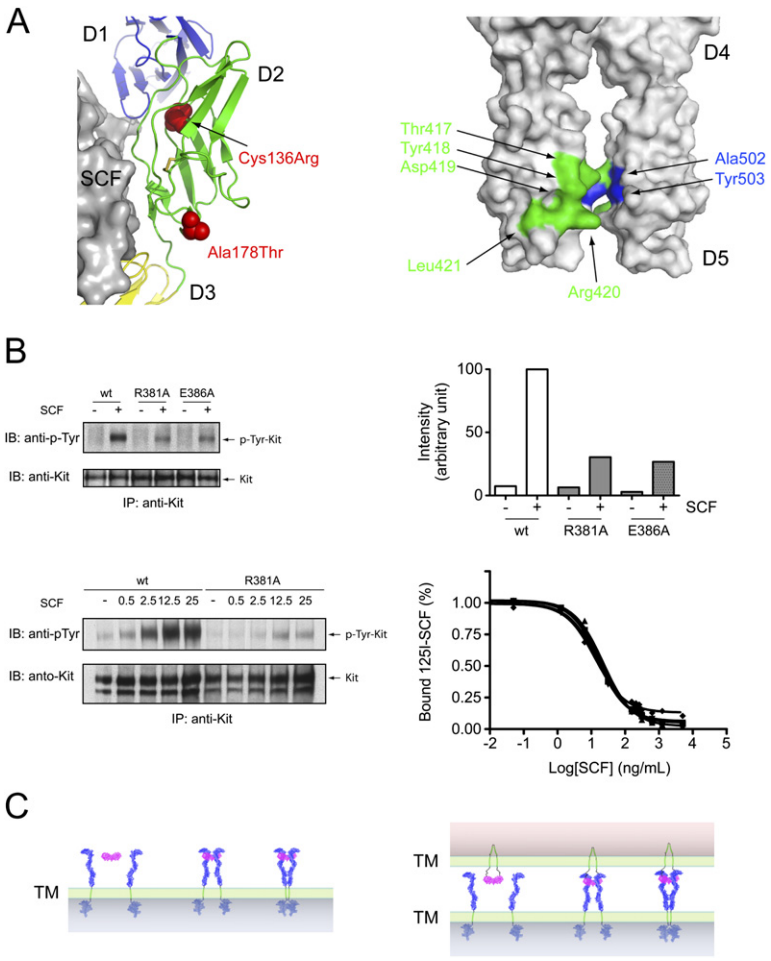

Figure 7. KIT Ectodomain Mutations Implicated in Cancer and Other Diseases and Mechanism of KIT and Other RTK Activation

(A) Loss-of-function mutations responsible for the piebald trait (left panel). A ribbon diagram of D1 (blue), D2 (green), and D3 (yellow) and a surface representation of SCF (gray) are shown. Mutated amino acids are colored in red. Gain-of-function mutations responsible for GIST, SCLC, and AML are shown (right panel). Surface representation of D4 and D5 in the homodimeric form is colored in gray. Ala502 and Tyr503 that are duplicated in GIST are shown in blue and deletions and insertional mutations in proximity to Asp419 (AML and NCLL) are shown in green. Note that the activating KIT mutations are confined to the D5-D5 interface.

(B) KIT activation is compromised by point mutants in D4-D4 interface. HEK293 cells transiently expressing wild-type KIT (WT), R381A, or E386A point mutations in D4 were stimulated with 10 ng/ml SCF for 6 min at 37°C as indicated (upper left panel). Lysates of unstimulated or SCF-stimulated cells were subjected to immunoprecipitation (IP) with anti-KIT antibodies followed by SDS-PAGE and immunoblotting (IB) with either anti-KIT or anti-phosphotyrosine (p-Tyr) antibodies. Densitometric quantitation of tyrosine autophosphorylation of KIT from anti-p-Tyr immunoblots (upper right panel). 3T3 cells stably expressing wild-type KIT (WT) or the R381A mutant were treated with different concentrations of SCF. Lysates from unstimulated or SCF-stimulated cells were subjected to immunoprecipitation with anti-KIT antibodies followed by SDS-PAGE and immunoblotting with anti-KIT or anti-p-Tyr antibodies (lower left panel). Displacement assay of cell-bound ^{125}I-SCF using native SCF. 3T3 cells expressing WT (■), R381A (▼), R381A/E386A (◆), or a kinase-negative KIT (▲) were treated with ^{125}I-SCF in the presence of increasing concentrations of native SCF. The EC50 (ligand concentration that displaces 50% of ^{125}I-SCF bound to c-KIT) of SCF toward WT KIT (1.1 nM) is comparable to the EC50 of SCF toward R381A (1.0 nM), R381A/E386A (0.8 nM), or the kinase-negative KIT mutant (1.4 nM).

(C) Models for KIT and other RTK activation driven by soluble (left panel) or membrane-anchored (right panel) SCF molecules expressed on the cell surface of a neighboring cell. SCF binding to the D1-D2-D3 ligand-binding module brings the C termini of the two bound KIT ectodomain monomers within 75 Å of each other. We propose that the flexibility of the D3-D4 and D4-D5 hinges enables lateral D4-D4 and D5-D5 interactions that bring the C termini of two neighboring ectodomains within 15 Å of each other. Consequently, the increased proximity and local concentration of KIT cytoplasmic domains leads to autophosphorylation of regulatory tyrosine residues in the kinase domain resulting in PTK activation. (Note that PTK activation is not drawn in the model.) Recruitment and activation of a complement of cell-signaling molecules will proceed following phosphorylation of key tyrosines in the cytoplasmic domain. The model is based on free SCF structure, ligand-free KIT, SCF-KIT complex, and KIT PTK structure (PDB entries 1QZJ, 1R01, and 1T45). Regions whose structures have not been determined were modeled using secondary structure prediction (green helices and black loops). SCF is colored in magenta, KIT ectodomain in blue, and KIT PTK in light blue.

Mechanism of Receptor Activation

The structures of KIT ectodomain monomers and SCF-induced dimers provide novel insights concerning the mechanism of ligand-induced activation of KIT and other RTKs containing five or seven Ig-like domains in their extracellular domains. Comparison of the structures of D1, D2, and D3 of KIT ectodomain monomers to the corresponding region in the SCF-induced ectodomain dimers shows very few structural alterations in the SCF-binding pocket and in other parts of D1, D2, and D3 following SCF binding. On the basis of their distinct biochemical functions, we have divided the ectodomain of KIT into three independent functional units. The first unit is composed of the three membrane-distal Ig-like domains D1, D2, and D3. The D1-D2-D3 region acts as a separate module that functions as a specific SCF binding unit. The SCF-binding unit is connected by a flexible joint (D3-D4 interface) to D4, a second independent unit that is connected by an additional flexible joint (D4-D5 interface) to D5, defined as a third independent unit. The function of D4

and D5 is to mediate, respectively, lateral D4-D4 and D5-D5 interactions that bring together and stabilize interactions between the membrane-proximal region of two neighboring KIT ectodomains.

According to this view, dimerization of KIT is driven by bivalent SCF binding whose sole function is to bind SCF and to bring together two KIT molecules. SCF-induced KIT dimerization is followed by a large change in D4 and D5 orientations relative to the position of the D1-D2-D3 SCF-binding unit. We propose that the flexible joints at the D3-D4 and D4-D5 interfaces enable lateral interactions that result in a large conformational change upon receptor dimerization. Rather than inducing a conformational change in KIT, dimerization may select particular conformations in a transition from a flexibly jointed monomer to a rigid dimer. This culminates in complex formations between two neighboring D4 and two neighboring D5 of KIT, bringing the C termini of D5 to a point at the cell membrane in which the transmembrane domains of two neighboring KIT molecules are within 15 Å of each other. Indeed, SCF-induced tyrosine autophosphorylation of KIT (Figure 7B) and stimulation of a downstream signaling pathways (data not shown) are strongly compromised by a point mutation in either Arg381 or Glu386 within D4 of KIT. PDGF-receptor activation and stimulation of downstream signaling pathways are also compromised by similar point mutations in D4 of PDGFR (Y.Y. and S.Y., unpublished data). We propose that the homotypic interactions between membrane-proximal regions of KIT are mediated primarily by the D4-D4 interface and that the D5-D5 interface plays a cooperative secondary role by facilitating exact positioning of two KIT ectodomains at the cell-surface interface.

The SCF-KIT complex exhibits strong polarization of the electrostatic field with the following characteristics: (1) an overall negatively charged surface; (2) complementarity between SCF (negative) and the ligand-binding D1-D2-D3 unit (positive); and (3) a strongly negatively polarized surface right above and around the D4-D4 interface (Figures 6D, 3B, and S6). We propose that the binding of SCF to KIT occurs in at least two steps: First, the electrostatic attraction between SCF and D1-D2-D3 will align SCF along the opposing ligand-binding region on KIT. The electrostatic attraction may also lead to a faster association rate of SCF due to a steering effect (Mueller et al., 2002). Subsequently, SCF-KIT complex formation will be stabilized by additional interactions including those mediated by a conformational change in bound SCF molecules. The strongly polarized electrostatic surface on D4 may also play a role in maintaining KIT in a monomeric inactive configuration by inducing repulsion between D4 domains of neighboring KIT receptors (Figure 6D). The binding affinities of D4 toward D4 and D5 toward D5 of neighboring receptors are probably too low to facilitate KIT ectodomain dimerization before the local receptor concentration on the cell surface is increased by SCF-driven receptor dimerization and by the effect of dimensionality. Once such a threshold of local concentration is reached, the attraction between neighboring D4 will overcome the electrostatic repulsion to the extent that two neighboring D4 units will be able to bind to each other. Interestingly, the main interactions that maintain the D4-D4 interface, i.e., double salt bridges between Arg381 and Glu386 in a neighboring KIT molecule are also mediated by electrostatic interactions.

The ectodomains of KIT and C-cadherin (Boggon et al., 2002) are each composed of five tandem Ig-like domains and both exhibit a similar elongated topology: 170 Å for KIT and 185 Å for C-cadherin. Moreover, the bacterial adhesion molecule invasin exhibits a remarkably similar elongated architecture and inter-Ig-like domain topologies (Hamburger et al., 1999). KIT ectodomains may have evolved from a common ancestral gene that coded for a protein that mediates cell-cell interactions. While classical cadherins utilize their most membrane-distal Ig-like domains for homotypic binding that mediates cell-cell interactions, the ectodomain of KIT has evolved to function as a cell-signaling receptor that binds membrane-anchored or soluble SCF isoforms to induce receptor dimerization and activation (Figure 7C).

Since the hallmarks of KIT structure, ligand binding, and receptor dimerization are conserved in other receptors, the mechanism described in this report for KIT activation may be a general mechanism for activation of many receptors (Figure 7C). Moreover, the structural information described in this report could be applied to design novel therapeutic interventions for treatment of cancers and other diseases driven by activated receptors.

EXPERIMENTAL PROCEDURES

Protein Expressions and Purifications

A soluble KIT ectodomain (amino acids 1–519) containing a polyhistidine tag at the C terminus was expressed in insect cells (Sf9) using the baculovirus expression system. KIT ectodomain was purified by Ni-chelate followed by size-exclusion chromatography (Superdex 200, GE Healthcare). After partial deglycosylation using endo-glycosidase F1, the ectodomain was further purified by anion exchange chromatography (MonoQ, GE Healthcare). SCF (1–141) was expressed, refolded, and purified as previously described (Langley et al., 1994; Zhang et al., 2000). Full details are described in Supplemental Experimental Procedures.

Crystallizations and Data Collections

Samples of KIT ectodomain alone or in complex with SCF were subjected to extensive screening for crystal growth and optimization. Crystals of deglycosylated ectodomain of approximate dimensions of 0.12 × 0.1 × 0.05 mm were obtained in phosphate buffer with polyethyleneglycol (PEG) as the precipitant (0.1 M Na-Pi buffer pH 6.0, 0.2 M KCl, 12% PEG 400) at 4°C. All crystals were immersed in a reservoir solution supplemented with 5%–18% glycerol for several seconds, flash cooled, and kept in a stream of nitrogen gas at 100 K during data collection. The crystals belonged to the rhomboidal space group *R*3 with unit cell dimensions of a = 162.4 Å, and c = 67.1 Å in hexagonal lattice setting, with one molecule per asymmetric unit. Platinum, bromine, and iodine derivatives of KIT were prepared by soaking the crystals in a reservoir solution containing heavy atom reagents in concentration ranges of 0.1 mM to 50 mM at 277 K for a few seconds to 10 days.

Crystals of the SCF-KIT complex were grown with PEG as the precipitant (0.2 M ammonium sulfate, 8%–12% PEG 8000, 5%–8% ethylene glycol at pH 7.0–8.5) at 4°C and diffraction data were collected to a resolution of 3.5 Å with a ADSD quantum-210 CCD detector at the X25 beamline of NSLS, Brookhaven National Laboratory. The crystals belong to the monoclinic space group *C*2, with unit cell dimensions a = 269.5 Å, b = 52.1 Å, c = 189.8 Å, β = 108.2°, which is comprised of two sets of SCF and KIT molecules in the asymmetric unit. All data sets were processed and scaled using the DENZO and SCALEPACK and the HKL2000 program package (Otwinowski and Minor, 1997). The data collection statistics are summarized in Table S3A.

Structure Determination

The experimental phases were calculated by using multiple isomorphous replacement with anomalous scattering (MIRAS) and by multiwavelength anomalous diffraction (MAD) to 3.0 Å resolution (Table S3A). The resulting electron-density maps showed continuous electron density of β sandwich structures and clear solvent-protein boundaries. The molecular model of monomeric KIT ectodomain was built manually into the experimental electron density maps. The structure was refined to 3.0 Å resolution using the native data set to a crystallographic R factor of 25.4% and free R factor of 29.6% (Table S3B). The structure of the SCF-KIT 2:2 complex was solved by molecular replacement using the structure of the monomeric form described in this report and the structure of SCF (Zhang et al., 2000; PDB code: 1EXZ) as search models. The structure was refined to 3.5 Å resolution using the native data set to a crystallographic R factor of 24.9% and free R factor of 29.5% (Tables S3A and S3B). Full details are described in Supplemental Experimental Procedures.

Molecular Graphics

Molecular images were produced using Pymol (http://pymol.sourceforge.net/) and CCP4MG (Potterton et al., 2004) software.

Cell Lines and Expression Vectors

Full details are described in Supplemental Experimental Procedures.

Supplemental Data

Supplemental Data include Experimental Procedures, six figures, and two movies and can be found with this article online at http://www.cell.com/cgi/content/full/130/2/323/DC1/.

ACKNOWLEDGMENTS

S.Y. was supported by a fellowship from the Uehara Memorial Foundation, and Y.O. is supported by a Cancer Research Institute postdoctoral fellowship. We thank Titus Boggon for valuable advice about the manuscript. This work was supported by NIH grants AR 051448, AR 051886, and P50 AR 054086. We thank Yoav Peleg from the Weizmann Institute for the GST-Endoglycosidase F1 plasmid and Brigitte D'arcy from Roche, Basel who provided the original plasmid. We also thank the staff of NSLS at beamlines X6A, X12B, X12C, X25, X26C, and X29.

Received: February 21, 2007
Revised: April 25, 2007
Accepted: May 22, 2007
Published: July 26, 2007

REFERENCES

Ashman, L.K. (1999). The biology of stem cell factor and its receptor C-kit. Int. J. Biochem. Cell Biol. *31*, 1037–1051.

Bernstein, A., Chabot, B., Dubreuil, P., Reith, A., Nocka, K., Majumder, S., Ray, P., and Besmer, P. (1990). The mouse W/c-kit locus. Ciba Found. Symp. *148*, 158–166.

Besmer, P., Lader, E., George, P.C., Bergold, P.J., Qiu, F.H., Zuckerman, E.E., and Hardy, W.D. (1986). A new acute transforming feline retrovirus with fms homology specifies a C-terminally truncated version of the c-fms protein that is different from SM-feline sarcoma virus v-fms protein. J. Virol. *60*, 194–203.

Blechman, J.M., Lev, S., Barg, J., Eisenstein, M., Vaks, B., Vogel, Z., Givol, D., and Yarden, Y. (1995). The fourth immunoglobulin domain of the stem cell factor receptor couples ligand binding to signal transduction. Cell *80*, 103–113.

Blume-Jensen, P., and Hunter, T. (2001). Oncogenic kinase signalling. Nature *411*, 355–365.

Boggon, T.J., Murray, J., Chappuis-Flament, S., Wong, E., Gumbiner, B.M., and Shapiro, L. (2002). C-cadherin ectodomain structure and implications for cell adhesion mechanisms. Science *296*, 1308–1313.

Copeland, N.G., Gilbert, D.J., Cho, B.C., Donovan, P.J., Jenkins, N.A., Cosman, D., Anderson, D., Lyman, S.D., and Williams, D.E. (1990). Mast cell growth factor maps near the steel locus on mouse chromosome 10 and is deleted in a number of steel alleles. Cell *63*, 175–183.

Flanagan, J.G., and Leder, P. (1990). The kit ligand: a cell surface molecule altered in steel mutant fibroblasts. Cell *63*, 185–194.

Fleischman, R.A., Saltman, D.L., Stastny, V., and Zneimer, S. (1991). Deletion of the c-kit protooncogene in the human developmental defect piebald trait. Proc. Natl. Acad. Sci. USA *88*, 10885–10889.

Fleischman, R.A., Gallardo, T., and Mi, X. (1996). Mutations in the ligand-binding domain of the kit receptor: an uncommon site in human piebaldism. J. Invest. Dermatol. *107*, 703–706.

Forbes, S., Clements, J., Dawson, E., Bamford, S., Webb, T., Dogan, A., Flanagan, A., Teague, J., Wooster, R., Futreal, P.A., and Stgratton, M.R. (2006). COSMIC 2005. Br. J. Cancer *94*, 318–322.

Greenwald, J., Vega, M.E., Allendorph, G.P., Fischer, W.H., and Choe, S. (2004). A flexible activin explains the membran-dependent cooperative assembly of TGF-β family receptors. Mol. Cell *15*, 485–489.

Halaby, D.M., Poupon, A., and Mornon, J. (1999). The immunoglobulin fold family: sequence analysis and 3D structure comparisons. Protein Eng. *12*, 563–571.

Hamburger, Z.A., Brown, M.S., Isberg, R.R., and Bjorkman, J. (1999). Crystal structure of invasin; a bacterial integrin-binding protein. Science *286*, 291–295.

Harpaz, Y., and Chothia, C. (1994). Many of the immunoglobulin superfamily domains in cell adhesion molecules and surface receptors belong to a new structural set which is close to that containing variable domains. J. Mol. Biol. *238*, 528–539.

Holden, H.M., Ito, M., Hartshorne, D.J., and Raymond, I. (1992). X-ray structure determination of telokin, the C-terminal domain of myosin light chain kinase, at 2.8Å resolution. J. Mol. Biol. *227*, 840–851.

Hsu, Y.R., Chang, W.C., Mendiaz, E.A., Hara, S., Chow, D.T., Mann, M.B., Langley, K.E., and Lu, H.S. (1998). Selective deamidation of recombinant human stem cell factor during in vitro aging: isolation and characterization of the aspartyl and isoaspartyl homodimers and heterodimers. Biochemistry *37*, 2251–2262.

Huang, E., Nocka, K., Beier, D.R., Chu, T.Y., Buck, J., Lahm, H.W., Wellner, D., Leder, P., and Besmer, P. (1990). The hematopoietic growth factor KL is encoded by the Sl locus and is the ligand of the c-kit receptor, the gene product of the W locus. Cell *63*, 225–233.

Jiang, X., Gurel, O., Mendiaz, E.A., Stearns, G.W., Clogston, C.L., Lu, H.S., Osslund, T.D., Syed, R.S., Langley, K.E., and Hendrickson, W.A. (2000). Structure of the active core of human stem cell factor and analysis of binding to its receptor kit. EMBO J. *19*, 3192–3203.

Langley, K.E., Mendiaz, E.A., Liu, N., Narhi, L.O., Zeni, L., Parseghian, C.M., Clogston, C.L., Leslie, I., Pope, J.A., Lu, H.S., et al. (1994). Properties of variant forms of human stem cell factor recombinantly expressed in Escherichia coli. Arch. Biochem. Biophys. *311*, 55–61.

Lemmon, M.A., Pinchasi, D., Zhou, M., Lax, I., and Schlessinger, J. (1997). Kit receptor dimerization is driven by bivalent binding of stem cell factor. J. Biol. Chem. *272*, 6311–6317.

Lev, S., Yarden, Y., and Givol, D. (1992). Dimerization and activation of the kit receptor by monovalent and bivalent binding of the stem cell factor. J. Biol. Chem. *267*, 15970–15977.

Mol, C.D., Dougan, D.R., Schneider, T.R., Skene, R.J., Kraus, M.L., Scheibe, D.N., Snell, G.P., Zou, H., Sang, B.C., and Wilson, K.P. (2004). Structural basis for the autoinhibition and STI-571 inhibition of c-Kit tyrosine kinase. J. Biol. Chem. *279*, 31655–31663.

Mueller, T.D., Zhanga, J.L., Sebalda, W., and Duschlb, A. (2002). Structure binding, and antagonists in the IL-4/IL-13 receptor systems. Biochim. Biophys. Acta *1592*, 237–250.

Murakami, T., Hosomi, N., Oiso, N., Giovannucci-Uzielli, M.L., Aquaron, R., Mizoguchi, M., Kato, A., Ishii, M., Bitner-Glindzicz, M., Barnicoat, A., et al. (2005). Analysis of KIT, SCF, and initial screening of SLUG in patients with piebaldism. J. Invest. Dermatol. *124*, 670–672.

Otwinowski, Z., and Minor, W. (1997). Processing of X-ray diffraction data collected in oscillation mode. Methods Enzymol. *276*, 307–326.

Philo, J.S., Wen, J., Wypych, J., Schwartz, M.G., Mendiaz, E.A., and Langley, K.E. (1996). Human stem cell factor dimer forms a complex with two molecules of the extracellular domain of its receptor, Kit. J. Biol. Chem. *271*, 6895–6902.

Potterton, L., McNicholas, S., Krissinel, E., Gruber, J., Cowtan, K., Emsley, P., Murshudov, G.N., Cohen, S., Perrakis, A., and Noble, M. (2004). Developments in the CCP4 molecular-graphics project. Acta Crystallogr. D Biol. Crystallogr. *60*, 2288–2294.

Ruch, C., Skiniotis, G., Steinmetz, M.O., Waltz, T., and Ballmer-Hofer, K. (2007). Structure of a VEGF-VEGF receptor complex determined by electron microscopy. Nat. Struct. Mol. Biol. *14*, 249–250.

Schlessinger, J. (2000). Cell signaling by receptor tyrosine kinases. Cell *103*, 211–225.

Su, X.D., Gastinel, L.N., Vaughn, D.E., Faye, I., Poon, P., and Bjorkman, P.J. (1998). Crystal structure of hemolin: a horseshoe shape with implications for homophilic adhesion. Science *281*, 991–995.

Tan, J.C., Nocka, K., Ray, P., Traktman, P., and Besmer, P. (1990). The dominant W42 spotting phenotype results from a missense mutation in the c-kit receptor kinase. Science *247*, 209–212.

Ullrich, A., and Schlessinger, J. (1990). Signal transduction by receptors with tyrosine kinase activity. Cell *61*, 203–212.

Vigers, G.P., Anderson, L.J., Caffes, P., and Brandhuber, B.J. (1997). Crystal Structure of type-I Interleukin-1 receptor complexed with interleukin-1βeta. Nature *386*, 190–194.

Zhang, Z., Zhang, R., Joachimiak, A., Schlessinger, J., and Kong, X.P. (2000). Crystal structure of human stem cell factor: implication for stem cell factor receptor dimerization and activation. Proc. Natl. Acad. Sci. USA *97*, 7732–7737.

Accession Numbers

The atomic coordinates and structure factors of KIT monomer and SCF-KIT complex have been deposited in the Protein Data Bank (http://www.rcsb.org/pdb) with accession codes 2EC8 and 2E9W, respectively.